Effect of fluid inertia on probe-tack adhesion

Eduardo O. Dias and José A. Miranda*

Departamento de Física, Universidade Federal de Pernambuco, Recife, PE 50670-901, Brazil

(Received 13 September 2011; revised manuscript received 14 December 2011; published 18 January 2012)

One way of determining the adhesive strength of liquids is provided by a probe-tack test, which involves measuring the force required to pull apart two parallel flat plates separated by a thin fluid film. The large majority of existing theoretical and experimental work on probe-tack adhesion use very viscous fluids and considers relatively low lifting plate velocities, so that effects due to fluid inertia can be neglected. However, the employment of low-viscosity fluids and the increase in operating speeds of modern lifting apparatus can modify this scenario. By dealing with a proper gap averaging of the Navier-Stokes equation, we obtain a modified Darcy-law-like description of the problem and derive an adhesion force which incorporates the effects of fluid inertia, fluid viscosity (for Newtonian and power law fluids), and the contribution of the compliance and inertia of the probe-tack apparatus. Our results indicate that fluid inertia may have a significant influence on the adhesion force profiles, inducing a considerable increase in the force peaks and producing oscillations in the force-displacement curves as the plate-plate separation is increased. The combined role of inertial and non-Newtonian fluid behaviors on the adhesion force response is also investigated.

DOI: 10.1103/PhysRevE.85.016312 PACS number(s): 47.50.−d, 47.15.gp, 68.35.Np, 68.15.+e

I. INTRODUCTION

During the past ten years or so, there has been continuously growing interest in the study of the adhesion properties of confined fluids [1–14]. A great variety of fluids have been used in these theoretical and experimental investigations ranging from simple Newtonian liquids, or more complicated non-Newtonian fluids (shear thinning, shear thickening, yield stress, etc.), through complex magnetic liquid suspensions (ferrofluids and magnetorheological fluids). One aspect in common in all these different studies is the necessity of evaluating and characterizing the bond strength of spatially constrained, liquid thin films. This is provided by the so-called probe-tack test [15,16].

In the plate-plate version of the probe-tack test, a fluid sample is placed between two parallel plane plates, and then the upper plate is lifted vertically at a known rate while the applied lifting force is recorded. The result of such measurement is a force-distance curve that quantifies the adhesive strength of the liquid sample as a function of the upper plate displacement. A typical force-distance curve usually starts with a sharp increase of the force once the probe is pulled apart. The force quickly reaches to its maximum and then drops asymptotically to zero as the plate-plate separation is increased. It has been shown [1–6] that the formation of a sharp peak is due to the compliance (natural elasticity) of the lifting apparatus.

In the context of probe-tack tests, the role of fluid inertia can be quantified by a Reynolds number (relative measure of inertial and viscous forces) which is directly proportional to the plate-plate separation and lifting plate velocity, and inversely proportional to the viscosity of the confined fluid sample. However, most experimental and theoretical studies in probe-tack adhesion [1–14] deal with very small separation gaps, relatively low lifting velocities, and highly viscous fluids. Under such circumstances, the vanishing Reynolds number limit is readily validated, and the effects of fluid inertia can be safely neglected. In this case, a standard lubrication approximation can be used, so that the fluid motion is perfectly described by Darcy's law, which connects the fluid velocity to the pressure gradient.

Although the assumption of negligible fluid inertia effects is entirely justified for the vast majority of studies in probe-tack adhesion, in certain situations it could be otherwise. The increase in operating speeds of modern lifting machines (varying from 1 to 40 mm/s) [4,6,17] and the possible use of fluids of low viscosity (for instance, water, mercury, or even some types of silicone oils [18]) could lead to a scenario in which fluid inertia can play a relevant role. Curiously, this state of affairs is quite similar to what recently happened in the area of viscous fingering pattern formation in Hele-Shaw cells [19,20]. Traditionally, inertial effects are not relevant to the Hele-Shaw flow problem. However, experimental [18] and theoretical [21–23] studies have demonstrated that if one utilizes fluids of low viscosity, larger Hele-Shaw plate spacings, and larger flow speeds, inertial effects play a key role in determining the dynamics and shape of the emerging fingering patterns. In this framework, the governing hydrodynamic equation is a modified, effectively two-dimensional (2D) Darcy's law based on a gap-averaging process of the three-dimensional (3D) Navier-Stokes equation, which includes the contribution of inertial terms [24–26].

Therefore, it would be of interest to evaluate the effect of fluid inertia on probe-tack tests and try to understand its influence on the force versus distance profiles. Even though the action of fluid inertia has been a vastly neglected topic in probe-tack adhesion, it has been analyzed by some investigators in the context of squeezing flows [27,28], involving Newtonian [29,30] and non-Newtonian [31] fluids. These theoretical studies [29–31] deal with a full Navier-Stokes equation and try, from first principles, to find an appropriate velocity profile for the flow problem. However, this constituted a quite challenging task due to the mathematical complexity of the hydrodynamic equations. For this reason, they had to approach the problem through perturbative methods or numerical computations. In

*jme@df.ufpe.br

spite of the relative intricacy of their models, they all concluded that fluid inertia can make a significant contribution to the squeezing force. In fact, a subsequent experimental work [32] has supported these theoretical findings by providing evidence that fluid inertia increases the force associated with both squeeze and pull-off flow processes.

Despite the significance and usefulness of the studies performed in Refs. [29–31], an alternative and simpler theoretical investigation of the influence of fluid inertia on probe-tack adhesion tests is still lacking. This is the problem we tackle in this work. We examine a model situation in which the confined fluid is either Newtonian or exhibits the simplest non-Newtonian rheology: a power law viscosity [27,33]. Within the approach originally proposed in Ref. [24], we consider a small Reynolds number, so that the velocity profile is solely determined by viscous effects and not altered by inertia. Additionally, we use a generalized velocity profile for non-Newtonian viscous effects related to a power law fluid, as proposed in Ref. [9]. These assumptions greatly simplify the solution of the probe-tack adhesion problem, leading to a gap-averaged nonlinear Darcy-like description. This allows the determination of the adhesion force, including fluid inertia and non-Newtonian contributions via analytic means. So, the relevance of these important physical factors on the force-distance profiles can be elucidated.

The layout of the rest of the paper is as follows: Sec. II presents our theoretical approach and derives the adhesion force between two flat parallel plates, taking into consideration the combined action of fluid inertia and non-Newtonian contributions. The introduction of the inertia and compliance of the probe-tack apparatus is also considered. A discussion about the role of fluid inertia in determining the force-distance profiles and the magnitude of the force peaks is presented in Sec. III. The Newtonian fluid limit is treated in Sec. III A, while the non-Newtonian (power law) case is discussed in Sec. III B. Our main results and conclusions are summarized in Sec. IV.

II. CALCULATION OF THE ADHESION FORCE INCLUDING FLUID INERTIA

A. Physical problem and constitutive equations

Figure 1 sketches the geometry of the probe-tack system. We consider a power law, incompressible fluid of viscosity η and density ρ located between two narrowly spaced parallel, flat plates. As in Refs. [1,3,5,8] we consider that the apparatus has a spring constant denoted by k. One end of the lifting apparatus moves at a specified constant velocity V, subjecting the upper plate to a pulling force F. The lower plate is held fixed at $z = 0$, where the z axis points in the direction perpendicular to the plates. The initial plate-plate distance is represented by b_0 and the initial fluid radius by R_0. At a given time t the plate spacing is $b = b(t)$, while the deformation due to the stretching of the apparatus is $L - b$, where $L = b_0 + Vt$. Note that due to the compliance of the measurement apparatus, the actual plate spacing b is not necessarily equivalent to L. Of course, in the case of a completely rigid apparatus we have $b = L$ and $\dot{b} = V$, where $\dot{b} = db/dt$.

Our main goal is to calculate the pulling force F as a function of displacement L, taking into account the effect

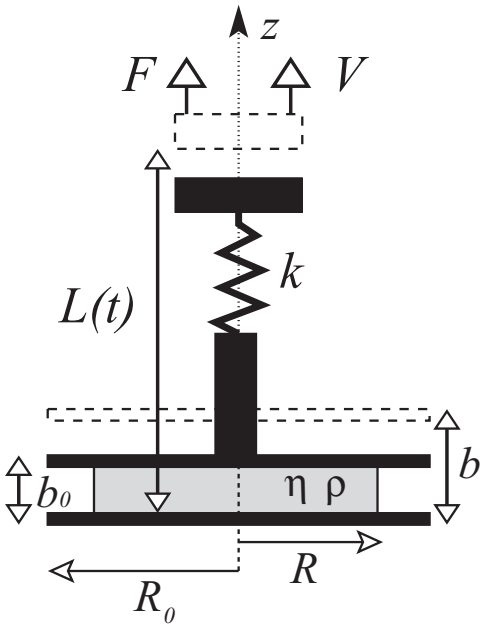

FIG. 1. Schematic representation of the probe-tack apparatus, where a fluid of viscosity η and density ρ is confined between parallel flat plates. While the lower plate remains at rest, the upper plate is lifted with constant velocity V through the application of a force F. The fluid's volume is kept constant during the lifting process so that $R^2 b = R_0^2 b_0$. The apparatus has elastic constant k and $L = b_0 + Vt$.

of fluid inertia. First, we calculate F analytically for the rigid case in order to maintain a given $b(t)$, and subsequently we address the situation in which compliance is taken into consideration by performing a numerical calculation. We follow Refs. [3] and [10] and derive F assuming that the fluid interface remains circular during the entire lifting process, with time-dependent radius defined as $R = R(t)$. Under such circumstances, conservation of fluid volume leads to the useful relation

$$R^2 b = R_0^2 b_0. \tag{1}$$

We start off by writing the governing equations of the problem in cylindrical polar coordinates (r,θ,z), namely the Navier-Stokes equation

$$\rho\left(\frac{\partial v_r}{\partial t} + v_r\frac{\partial v_r}{\partial r} + v_z\frac{\partial v_r}{\partial z}\right) = -\frac{\partial p}{\partial r} + \frac{\partial}{\partial z}\left(\eta\frac{\partial v_r}{\partial z}\right) \tag{2}$$

and the continuity equation for incompressible fluids

$$\frac{1}{r}\frac{\partial(r v_r)}{\partial r} + \frac{\partial v_z}{\partial z} = 0, \tag{3}$$

where $v_r = v_r(r,z)$ and $v_z = v_z(r,z)$ are the 3D velocity components in the radial and axial directions, respectively. Note that in the axisymmetric flow considered here only the radial and axial components of the velocity are nonvanishing, so that the azimuthal component of the velocity v_θ is null. Here p denotes the hydrodynamic pressure. The left-hand side of Eq. (2) contains the inertial terms, while the right-hand side incorporates contributions from pressure and viscous stresses. As in Refs. [9,24], we focus on a high-aspect-ratio situation (thin gap compared to any in-plane dimension, or $R/b \gg 1$),

so that the dominant shear is given by $\partial v_r/\partial z$. For such a confined flow, gravity effects can be safely neglected [1–6].

We consider a power law fluid of viscosity

$$\eta(a) = \eta_0 \left| \frac{\partial v_r}{\partial z} \right|^a, \tag{4}$$

where the exponent a expresses the non-Newtonian nature of the fluid under tension: $a = 0$ corresponds to the Newtonian fluid limit, while $a < 0$ ($a > 0$) describes the shear-thinning (shear-thickening) situation. Of course, when $a = 0$, $\eta(0)$ is the Newtonian viscosity.

Existing rheological experiments [33] using solutions of xanthane (a stiff rod-like polymer) are able to determine both the power law index a and the consistency parameter η_0 for different polymer concentrations. As shown in Ref. [33], these laboratory measurements are satisfactorily described by the expression (4), where the viscosity shows a power law dependence on the shear rate. Moreover, experiments performed by Leider [34] using various polymeric fluids [including silicone and polyisobutylene (PIB) fluids] found that the power law model was indeed very appropriate to describe the rheological behavior of such materials.

B. Velocity approach

Finding a closed-form solution of a partial differential equation like the one shown in Eq. (2) is definitely not an easy task. Instead of trying to solve Eq. (2) by using standard perturbation techniques or brute force numerical schemes [29–31], here we employ an alternative approach. We closely follow the procedure originally proposed in Refs. [9,24], which consider a trial velocity solution

$$v_r(r,z) = f(r)g(z), \tag{5}$$

where

$$g(z) = \left| z - \frac{b}{2} \right|^\alpha - \left(\frac{b}{2} \right)^\alpha, \tag{6}$$

with $\alpha = (a+2)/(a+1)$. The central idea behind this ansatz is the consideration that velocity profile given by Eq. (6) (see also Eq. (5) in Ref. [9]) holds provided a low-Reynolds-number and high-aspect-ratio situation under moderate shear is assumed. These are precisely the circumstances which pertain to our problem. Notice that the standard parabolic velocity profile is immediately recovered from Eq. (6) in the Newtonian limit.

As in Refs. [9,24], we proceed by adopting a Darcy-law-like approach and focus on the gap-averaged value of the radial velocity

$$u_r = u_r(r) = \frac{1}{b} \int_0^b v_r(r,z)dz. \tag{7}$$

By substituting Eqs. (5) and (6) into (7), we obtain that

$$f(r) = -\frac{2^\alpha(1+\alpha)}{b^\alpha \alpha} u_r(r). \tag{8}$$

Note that the explicit r dependence of $f(r)$ can be obtained by taking the time derivative of the volume conservation expression (1), leading to

$$u_r(r) = \dot{R} = -\frac{\dot{b}}{2b} r, \tag{9}$$

which relates the upper plate and the interface velocities.

C. Darcy-like equation and the adhesion force

With $g(z)$ expressed by Eq. (6) and $f(r)$ given by Eq. (8), we are ready to obtain a Darcy-law-like equation for the problem. Following the standard approach used in Hele-Shaw problems [20] and fluid adhesion problems in confined plate-plate geometry [1–14], we take the gap average of Eq. (2) and use Eq. (8) to express the resulting equation in terms of u_r. As a result of such gap-averaging process, a nonlinear generalized Darcy-like equation is obtained:

$$\rho \left[\frac{\partial u_r}{\partial t} + \frac{\dot{b}}{b} u_r + \frac{(4a+6)}{(3a+5)} \left(2u_r \frac{\partial u_r}{\partial r} + \frac{u_r^2}{r} \right) \right] = -\frac{\partial p}{\partial r} + \frac{2\eta_0}{b^{a+2}} \left(\frac{4a+6}{a+1} \right)^{a+1} |u_r|^{a+1}. \tag{10}$$

Details about the derivation of Eq. (10) are presented in the appendix. Notice that the usual Darcy's law [19,20] for Newtonian fluids ($a = 0$) is recovered when inertial terms on the left-hand side of (10) are entirely disregarded.

By substituting Eq. (9) into Eq. (10) and integrating, the pressure field can be written as

$$p(r) = p_0 + \rho \left[\frac{\ddot{b}}{4b} - \frac{3}{8} \frac{(4a+6)}{(3a+5)} \frac{\dot{b}^2}{b^2} \right] (r^2 - R^2) + \frac{2\eta_0}{(a+2)} \frac{\dot{b}^{a+1}}{b^{2a+3}} \left(\frac{2a+3}{a+1} \right)^{a+1} (r^{a+2} - R^{a+2}), \tag{11}$$

where p_0 is the atmospheric pressure in the region outside the fluid droplet. As is common in this type of adhesion phenomenon, surface tension effects can be neglected [1–6].

The force exerted by the lifting machine on the upper plate is calculated by integrating the pressure [Eq. (11)] over the area occupied by the fluid $F = \int_0^R [p_0 - p(r)] 2\pi r dr$, leading to

$$F = \frac{\rho\pi R_0^4 b_0^2}{8} \left[\frac{\ddot{b}}{b^3} - \frac{(6a+9)}{(3a+5)} \frac{\dot{b}^2}{b^4} \right] + \frac{2\pi\eta_0 R_0^{a+4} b_0^{\frac{a}{2}+2}}{a+4} \left(\frac{2a+3}{a+1} \right)^{a+1} \frac{\dot{b}^{a+1}}{b^{\frac{5a}{2}+5}}. \tag{12}$$

Similar to what is done in Refs. [1,3,7,8], a convenient dimensionless expression for Eq. (12) can be obtained by rescaling lengths by $\delta = [3\pi\eta(0)R_0^4 b_0^2 V/2k]^{1/6}$ and velocities by V, resulting in

$$F = \mathrm{Re} \left[\frac{\ddot{b}}{b^3} - \frac{(6a+9)}{(3a+5)} \frac{\dot{b}^2}{b^4} \right] + \mathcal{N}(a) \frac{\dot{b}^{a+1}}{b^{\frac{5a}{2}+5}}, \tag{13}$$

where fluid inertia effects are accounted for by a Reynolds number

$$\mathrm{Re} = \frac{\rho V \delta}{12\eta(0)}, \tag{14}$$

and

$$\mathcal{N}(a) = \frac{4}{3(a+4)}\left(\frac{2a+3}{a+1}\right)^{a+1}\left(\frac{V R_0\sqrt{b_0}}{\delta^{5/2}}\right)^{a} \tag{15}$$

represents a non-Newtonian parameter. From now on we work with the dimensionless version of the problem. It is worth mentioning that if we deal with constant lifting velocity, we have $b = L$ and hence $\dot{b} = 1$. Equation (13) shows $\dot{b}$ and $\ddot{b}$ explicitly in anticipation of our analysis of the compliant apparatus situation. Note that when $\mathrm{Re} = 0$ and $a = 0$ [$\mathcal{N}(0) = 1$] Eq. (13) reduces to the inertialess, Newtonian situation [3]. On the other hand, when $\mathrm{Re} = 0$, $a \neq 0$, and with dimensions properly reintroduced, the inertialess case for power law fluids is recovered [27].

As commented at the beginning of this work, typical force-distance curves increase sharply during the initial stages of the plate-separation process. This effect is not described by the hydrodynamic forces within the fluid but is a result of the elasticity of the apparatus [1,3,4]. We conclude this section by discussing a way to access the complete form of the force-distance curves, including the inertial and viscous properties of the fluid, plus the intrinsic flexibility, as well as the inertia of the lifting machine. To accomplish this, we adapt a method originally developed by Francis and Horn [1] for their sphere-plate geometry with Newtonian liquids for inertialess fluid and apparatus.

It is assumed that, during the entire separation process, there is an interplay among fluid inertia, viscous, and the spring-restoring (dimensionless) force $L - b$ which results from the deflection of the apparatus. The influence of the apparatus inertia can be evaluated by incorporating an acceleration term into this dynamic scenario. Taking all this into account and utilizing Eq. (13), we obtain a nonlinear second-order differential equation for $b = b(t)$

$$(L-b) - \left\{\mathrm{Re}\left[\frac{\ddot{b}}{b^3} - \frac{(6a+9)}{(3a+5)}\frac{\dot{b}^2}{b^4}\right] + \mathcal{N}(a)\frac{\dot{b}^{a+1}}{b^{\frac{5a}{2}+5}}\right\} = M\ddot{b}, \tag{16}$$

where $M = mV^2/k\delta^2$ is the dimensionless mass of the apparatus. We solve Eq. (16) numerically for $b(t)$, use the dimensionless relation $L = b_0 + t$ to write b as a function of L, and subsequently obtain the pulling force $F = L - b$. We utilize differential equation (16) to obtain the complete force-distance profiles.

In order to strengthen the practical and academic relevance of our theoretical study, we ensure that the values of all relevant dimensionless quantities we utilize are consistent with realistic physical parameters related to existing probe-tack test instruments [1–6] and material properties of the fluids [3,9,18]. We understand this could make our work of broader interest and eventually help experimentalists test the predictions of our theoretical model.

III. EFFECT OF FLUID INERTIA

A. Newtonian case

We begin our discussion by examining the effect of fluid inertia on force-displacement (F vs L) curves of Newtonian fluids ($a = 0, \mathcal{N} = 1$). Figure 2 plots F vs L considering the combined influence of fluid inertia (controlled by Re) and the inertial contribution from the apparatus itself (M) for $b_0 = 1.7$. In both Figs. 2(a) and 2(b), the dashed curves represent the situation in which inertial effects are completely neglected ($\mathrm{Re} = 0$ and $M = 0$). On the other hand, the black solid curves indicate the sole influence of the fluid inertia ($\mathrm{Re} = 0.02$ and $M = 0$), while the gray solid curves depict the circumstances in which fluid and apparatus inertia act simultaneously ($\mathrm{Re} = 0.02$ and $M \neq 0$).

By inspecting Fig. 2, it is evident that fluid inertia significantly increases the force peak (difference between black solid and dashed curves). Physically, this is justified by the resistance

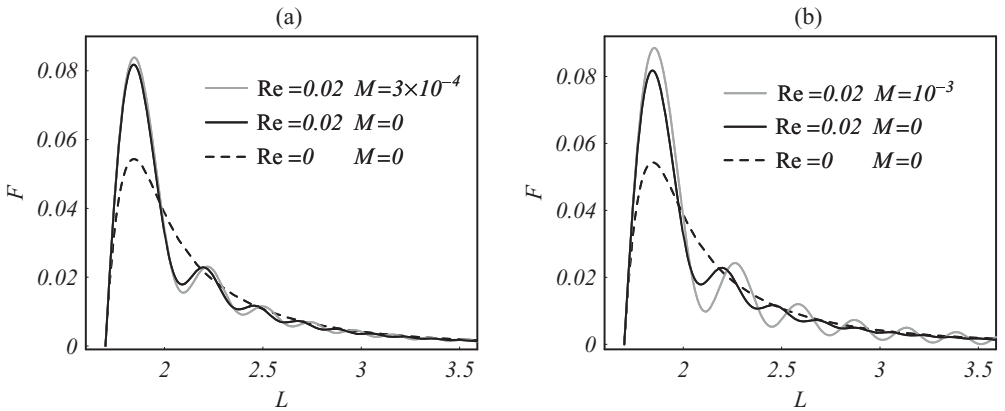

FIG. 2. Adhesion force F as a function of displacement L considering the role of fluid inertia (Re) and the inertia of the apparatus (M) in the Newtonian limit $a = 0$. In (a), the value of M is taken from typical parameters used in real probe-tack experiments [1–6,14]. In (b), the value of M has been exaggerated in order to highlight the influence of the inertia of the instrument. It can be seen that fluid inertia leads to a significant increase of the adhesion force peak, followed by oscillations which become less intense for larger L. Conversely, oscillations tend to persist if apparatus inertia is overestimated. Here the initial plate separation $b_0 = 1.7$.

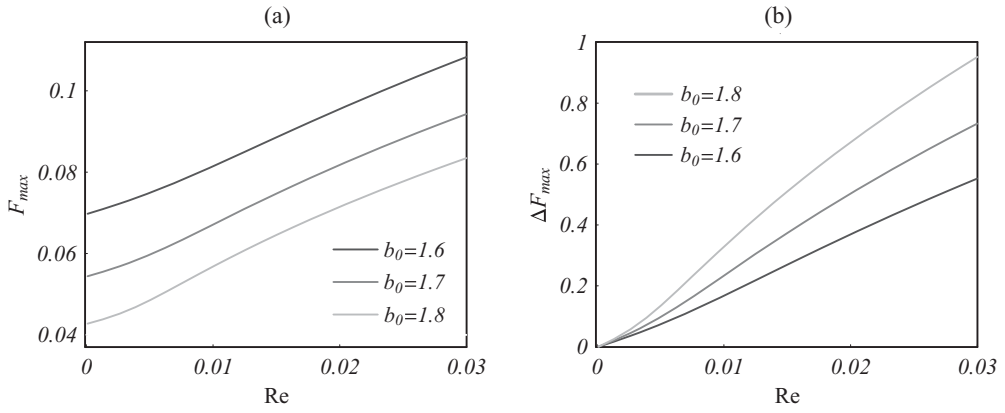

FIG. 3. (a) Maximum value of the adhesion force $F_{\max}$ as a function of the Reynolds number Re. (b) Relative growth $\Delta F_{\max}$ [as defined by Eq. (17)] plotted with respect to changes in Re. Three different values of b_0 are considered: 1.6, 1.7, and 1.8.

against motion due to the fluid inertia term proportional to the acceleration on the left-hand side of Eq. (16). It is also noticeable that fluid inertia induces oscillations in the force curves, which tend to die out rapidly as L is increased.

Moreover, it is interesting to contrast the different roles played by fluid inertia and apparatus inertia. In Fig. 2(a), the gray curve is plotted by taking a value of M which considers typical experimental parameters for usual probe-tack tests (apparatus of a few hundred grams) [1–6,14]. It is readily observed that the effect of the apparatus inertia is negligible if compared with the impact of fluid inertia. To access more visible effects from the apparatus inertia, we exaggerate the value of M in Fig. 2(b). In this case, we notice a small increase in the force peak, accompanied by the development of more intense oscillations, which still remain sizable at the curve's tail. This behavior can be understood from Eq. (16) by identifying the total acceleration term as $[M + \mathrm{Re}/b^3]\ddot{b}$, which is mainly responsible for the curve oscillations. So, while the fluid inertia term decays with increasing plate separation ($\sim 1/b^3$), the apparatus inertia term is independent of b. This justifies why the oscillations due to the apparatus inertia tend to survive for a longer time when M is considerably augmented. Notice that for the noncompliant case (rigid apparatus), the force-distance curves of Fig. 2 would not display peaks and curve oscillations.

It is worth noting that the negligible role of the apparatus inertia has already been pointed out in Ref. [2]. However, the influence of fluid inertia on the shape of the F vs L curves and the relative importance of fluid and apparatus inertia have not been examined. From this point on, the effects of the apparatus inertia will be neglected.

We proceed by examining how the maximum of the adhesion force $F_{\max}$ varies with the Reynolds number Re for different values of the initial plate separation b_0 [Fig. 3(a)]. $F_{\max}$ is increased for increasingly larger values of Re. Despite of the fact that smaller values of b_0 lead to larger magnitudes of $F_{\max}$, the rate of change of $F_{\max}$ with respect to Re is practically the same, regardless the value of b_0. At first glance this may sound a bit counterintuitive, since one could expect stronger inertial effects for larger initial place separations. To investigate this point a bit further, we evaluate how the relative growth of $F_{\max}$

$$\Delta F_{\max} = \frac{F_{\max}(\mathrm{Re}) - F_{\max}(\mathrm{Re}=0)}{F_{\max}(\mathrm{Re}=0)} \tag{17}$$

changes with the Reynolds number. This is done in Fig. 3(b) for the same values of b_0 utilized in Fig. 3(a). It is now clear that larger b_0 values result in stronger growth of $\Delta F_{\max}$ with Re. For instance, for $b_0 = 1.8$ the force peak grows almost 100% in the interval $0 \leqslant \mathrm{Re} \leqslant 0.03$. This is a clear indicator of the significant impact of fluid inertia on the adhesive strength of confined liquids for this range of Re.

B. Non-Newtonian case

In this section, we turn to the influence of fluid inertia on the adhesion force when the non-Newtonian nature of the liquid is taken into account. Figure 4 plots the force-displacement curves for $b_0 = 1.6$ and three values of the power law exponent a: 0.03 (dark gray curve), 0 (dashed curve), and -0.03

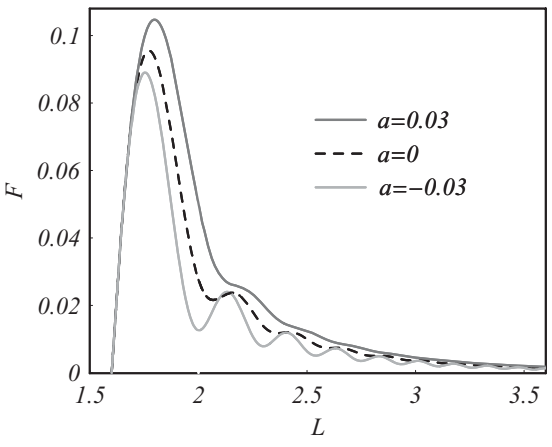

FIG. 4. Adhesion force F as a function of displacement L for three different values of the power law exponent a and the non-Newtonian parameter $\mathcal{N}(a)$: 0.03 and $\mathcal{N}(0.03) = 1.31$ (shear-thickening case), 0 and $\mathcal{N}(0) = 1$ (Newtonian limit), and -0.03 and $\mathcal{N}(-0.03) = 0.76$ (shear-thinning case). Here $\mathrm{Re} = 0.02$ and $b_0 = 1.6$.

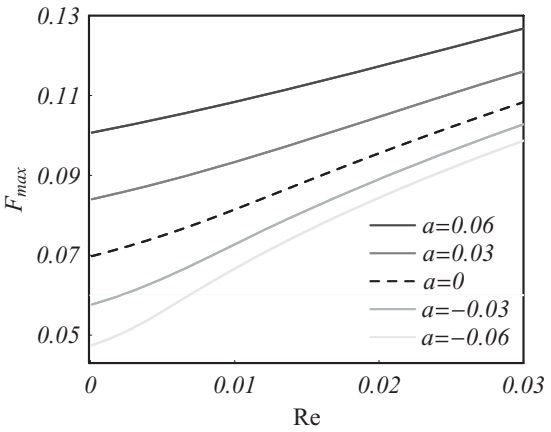

FIG. 5. (a) Maximum value of the adhesion force $F_{\max}$ as a function of the Reynolds number Re, for five different values of the power law exponent a.

(light gray curve). For a shear-thinning fluid ($a = -0.03$), we observe a decrease in the magnitude of the force peak with respect to the Newtonian situation. This indicates a reduced adhesion behavior for shear-thinning fluids. However, we also notice that curve oscillations become more intense. On the other hand, for a shear-thickening fluid ($a = 0.03$) we verify the opposite behavior, so that the force peak is increased if contrasted with the Newtonian peak position, but curve oscillations are attenuated.

These behaviors are a result of an interplay between inertial and viscous contributions: When $a = -0.03$, the effective viscosity decreases during the lifting process, leading to a lower viscous resistance and causing a lower peak position. In addition, after the peak is formed, stronger inertial effects become prevalent, inducing more intense oscillations. The same type of explanation is valid for the $a = -0.03$ case, where larger effective viscosity produces a higher force peak and damps curve oscillations.

We close this section by examining Fig. 5, which depicts the maximum value of the adhesion force $F_{\max}$ as a function of the Reynolds number Re for five different values of a, and $b_0 = 1.6$. The dashed curve (Newtonian case) in Fig. 5 is precisely the dark gray curve plotted in Fig. 3, but now we fix b_0 and focus on the influence of a on the behavior of $F_{\max}$ as the fluid inertia is modified. We can verify that larger negative values of a (lighter gray curves) induce a more significant change of $F_{\max}$ as fluid inertia is increased. Consequently, the different curves tend to converge when Re gets larger. In other words, a more intense inertial contribution tends to inhibit the capability of the non-Newtonian effects to alter the adhesive strength of the fluid.

IV. SUMMARY AND CONCLUSION

A typical procedure to characterize the adhesive strength of a fluid is performed by a tensile test (i.e., a probe-tack test), which measures the force required to pull apart two surfaces bonded by a thin liquid film. In most probe-tack adhesion studies to date, both separation gaps and lifting velocities are small, and the fluids used are highly viscous. Under such circumstances, inertial effects are indeed negligible. However, the action of fluid inertia can become significant if larger plate spacing, low viscosity fluids, and higher pulling-off velocities are used. Despite the feasibility of a regime in which fluid inertia is important to adhesion force measurements and calculations, this research topic has been relatively ignored.

In this work, we studied the influence of fluid inertia on the adhesive performance of Newtonian and power law fluids under tension. Our theoretical analysis is performed through a gap-averaged Darcy-law-like version of the hydrodynamic problem, in a low-Reynolds-number limit. For a rigid probe-tack apparatus, the adhesion force is derived analytically by taking into account fluid inertia and viscosity effects. The influence of the compliance of the measurement apparatus as well as its own inertia is considered and analyzed by a numerical solution of a nonlinear differential equation for the force profile.

If the confined fluid is Newtonian, our results indicate that fluid inertia makes a significant contribution to the adhesion force. It alters the force profile at early stages of plate separation by considerably increasing the magnitude of the force peak. In addition, after the maximum force is reached, fluid inertia induces relatively mild oscillations that tend to attenuate at the tail of the force-distance curves. We have also shown that under usual circumstances, the inertia of the apparatus just adds a very small correction to the probe-tack measurements, being negligible if compared to the strength of the fluid inertia contribution.

Similar kind of findings (considerable increase in the force peak followed by curve oscillations) are verified in the case of non-Newtonian, power law fluids. Here a competition between fluid inertia and non-Newtonian viscous properties determines the force versus gap profile. If shear rates cause the power law liquid to shear thin to a viscosity below that for the Newtonian liquid limit (i.e., $a = 0$), a lower maximum force results and stronger oscillations arise at the curve's tail. The opposite behavior is observed for shear-thickening fluids, where the maximum force is larger than that for the Newtonian liquids, and curve oscillations are considerably damped. Artificially enlarged apparatus inertia effects would not vary much the force peak but would lead to more intense oscillations at the curve's tail. So, contrary to the typical action of fluid inertia, larger inertia of the instrument would induce persistent oscillations even at the tail of the force-displacement curves.

More insight about probe-tack adhesion in the regime where fluid inertia is relevant should be gained from experiments and further analytical or numerical descriptions of the flow characteristics. Maybe one could consider more complicated situations in which cavitation, different surface types, slip, elastic effects, pinning of the contact line, etc., might play some role. Consideration of more complex non-Newtonian behaviors such as the ones presented by yield-stress fluids and shear-thinning fluids with Newtonian plateau would also be of interest. We hope our work will motivate investigators to examine these suggestive adhesion research topics.

ACKNOWLEDGMENT

We thank CNPq for financial support through the program "Instituto Nacional de Ciência e Tecnologia de Fluidos

Complexos (INCT-FCx)" and also through the CNPq/FAPESQ Pronex program.

APPENDIX: DARCY-LIKE LAW

This appendix presents details of the derivation of Eq. (10). We begin by presenting the gap average calculation of each term in Eq. (2), using the velocity solution $v_r(r,z) = f(r)g(z)$ [Eq. (5)]. The gap average of the first two terms on the left-hand side of Eq. (2) are

$$\frac{1}{b}\int_0^b \frac{\partial v_r}{\partial t}dz = \frac{1}{b}\frac{\partial f(r)}{\partial t}\int_0^b g(z)dz, \qquad \text{(A1)}$$

$$\frac{1}{b}\int_0^b v_r\frac{\partial v_r}{\partial r}dz = \frac{1}{b}f(r)\frac{\partial f(r)}{\partial r}\int_0^b [g(z)]^2dz. \qquad \text{(A2)}$$

The third term on the left-hand side of Eq. (2) can be written as

$$\frac{1}{b}\int_0^b v_z\frac{\partial v_r}{\partial z}dz = \left(\frac{1}{b}\right)(v_r v_z)\Big|_{z=0}^{z=b} - \frac{1}{b}\int_0^b v_r\frac{\partial v_z}{\partial z}dz.$$

Note that the piece involving $v_r v_z$ is zero, since $v_r(r,0) = v_r(r,b) = 0$. Moreover, by using the incompressibility condition (3), the remaining term can be rewritten as

$$\frac{1}{b}\int_0^b \frac{v_r}{r}\frac{\partial(r v_r)}{\partial r}dz = \frac{1}{b}\frac{f(r)}{r}\frac{\partial[rf(r)]}{\partial r}\int_0^b [g(z)]^2dz. \qquad \text{(A3)}$$

For the confined geometry of the probe-tack problem, the pressure is considered to be nearly constant in the gap direction, so that the gap average of the first term on the right-hand side of (2) is trivial. On the other hand, the gap average of the second term on the right-hand side of Eq. (2) is

$$\frac{1}{b}\int_0^b \frac{\partial}{\partial z}\left(\eta\frac{\partial v_r}{\partial z}\right)dz = \frac{1}{b}\eta\frac{\partial v_r}{\partial z}\Big|_{z=0}^{z=b}$$

$$= \frac{2}{b}\eta_0[f(r)]^{a+1}\left[\frac{\partial g(z)}{\partial z}\right]^{a+1}\Big|_{z=b}, \qquad \text{(A4)}$$

where we have utilized the power law fluid viscosity expression (4). At this point, notice that Eqs. (A1)–(A4) are conveniently written in terms of the functions $g(z)$ and $f(r)$. The rest of the derivation consists of substituting Eqs. (6) and (8) into Eqs. (A1)–(A4), and explicitly evaluating simple derivatives and integrals. This procedure yields the Darcy-like law equation (10) of the text.

[1] B. A. Francis and R. G. Horn, J. Appl. Phys. **89**, 4167 (2001).
[2] B. A. Francis, Ph.D. thesis, University of South Australia, 1999 (unpublished).
[3] D. Derks, A. Lindner, C. Creton, and D. Bonn, J. Appl. Phys. **93**, 1557 (2003).
[4] M. Tirumkudulu, W. B. Russel, and T. J. Huang, Phys. Fluids **15**, 1588 (2003).
[5] S. Poivet, F. Nallet, C. Gay, and P. Fabre, Europhys. Lett. **62**, 244 (2003).
[6] S. Poivet, F. Nallet, C. Gay, J. Teisseire, and P. Fabre, Eur. Phys. J. E **15**, 97 (2004).
[7] J. A. Miranda, Phys. Rev. E **69**, 016311 (2004).
[8] J. A. Miranda, R. M. Oliveira, and D. P. Jackson, Phys. Rev. E **70**, 036311 (2004).
[9] M. Ben Amar and D. Bonn, Phys. D (Amsterdam, Neth.) **209**, 1 (2005).
[10] A. Lindner, D. Derks, and M. J. Shelley, Phys. Fluids **17**, 072107 (2005).
[11] J. Nase, A. Lindner, and C. Creton, Phys. Rev. Lett. **101**, 074503 (2008).
[12] S. A. Lira and J. A. Miranda, Phys. Rev. E **80**, 046313 (2009).
[13] Q. Barral, G. Ovarlez, X. Chateau, J. Boujlel, B. Rabideau, and P. Coussot, Soft Matter **6**, 1343 (2010).
[14] R. H. Ewoldt, P. Tourkine, G. H. McKinley, and A. E. Hosoi, Phys. Fluids **23**, 073104 (2011).
[15] A. Zosel, Colloid Polym. Sci. **263**, 541 (1985).
[16] H. Lakrout, P. Sergot, and C. Creton, J. Adhes. **69**, 307 (1999).
[17] J. Chen, M. Feng, Y. Gonzalez, and L. A. Pugnaloni, J. Food Eng. **87**, 281 (2008).
[18] C. Chevalier, M. Ben Amar, D. Bonn, and A. Lindner, J. Fluid Mech. **552**, 83 (2006).
[19] P. G. Saffman and G. I. Taylor, Proc. R. Soc. London A **245**, 312 (1958).
[20] G. M. Homsy, Annu. Rev. Fluid Mech. **19**, 271 (1987); K. V. McCloud and J. V. Maher, Phys. Rep. **260**, 139 (1995); J. Casademunt, Chaos **14**, 809 (2004).
[21] A. He and A. Belmonte, J. Fluid Mech. **668**, 436 (2011).
[22] E. O. Dias and J. A. Miranda, Phys. Rev. E **83**, 046311 (2011).
[23] E. O. Dias and J. A. Miranda, Phys. Rev. E **83**, 066312 (2011).
[24] P. Gondret and M. Rabaud, Phys. Fluids **9**, 3267 (1997).
[25] C. Ruyer-Quil, C. R. Acad. Sci. Paris IIb **329**, 337 (2001).
[26] F. Plouraboue and E. J. Hinch, Phys. Fluids **14**, 922 (2002).
[27] R. B. Bird, R. Armstrong, and O. Hassager, *Dynamics of Polymeric Liquids* (Wiley, New York, 1977).
[28] J. Engmann, C. Servais, and A. S. Burbidge, J. Non-Newtonian Fluid Mech. **132**, 1 (2005).
[29] S. Ishizawa, Bull. J. Soc. Mech. Eng. **9**, 533 (1966).
[30] D. C. Kuzma, Appl. Sci. Res. **18**, 15 (1967).
[31] G. Ramanaiah, Appl. Sci. Res. **18**, 183 (1967).
[32] D. R. Oliver and M. Shahidullah, J. Non-Newtonian Fluid Mech. **15**, 331 (1984).
[33] A. Lindner, D. Bonn, and J. Meunier, Phys. Fluids **12**, 265 (2000).
[34] P. J. Leider, Ind. Eng. Chem. Fundam. **13**, 342 (1974).